ACS Partner Journal

POLYMER SCIENCE & TECHNOLOGY

https://pubs.acs.org/PolySciTech

Article

CD7-Specific Polymersomal Vincristine Delivery Potentiates Chemotherapy in T-Cell Acute Lymphoblastic Leukemia

Published as part of Polymer Science & Technology special issue "Biomedical Polymers".

Zhenzhen Zhai,[#] Yifan Zhang,[#] Shujing Yue, Fengtao You, Lin Yang, Zhiyuan Zhong,* and Huanli Sun*

Cite This: https://doi.org/10.1021/polymscitech.5c00030

Read Online

ACCESS | Metrics & More | Article Recommendations | Supporting Information

ABSTRACT: T-cell acute lymphoblastic leukemia (T-ALL) is an invasive hematological malignancy characterized by a high relapse rate, due to the lack of targeted therapies. Despite intensive chemotherapy having advanced treatment progress, most patients experience treatment failure and endure severe side effects. Here, a CD7-specific polymersomal vincristine delivery system was engineered on the basis of anti-CD7 nanobody-conjugated chimeric polymersomes (aCD7P-VCR) for targeted chemotherapy of T-ALL. aCD7P-VCR, with tunable aCD7 nanobody density, mediated selective targeting and potent inhibition of CD7-positive CCRF-CEM T-ALL cells, resulting in a half-maximal inhibitory concentration of 0.11 nM VCR, but caused no obvious toxicity to normal peripheral blood mononuclear cells or T cells at 10.8 nM VCR. Interestingly, aCD7P-VCR treatment substantially reduced leukemia progression and invasion in the orthotopic CCRF-CEM T-ALL model without toxic effects, leading to significantly longer survival than clinically used VCR and nontargeted P-VCR. aCD7P-VCR is expected to provide an effective and targeted therapeutic approach for T-ALL.

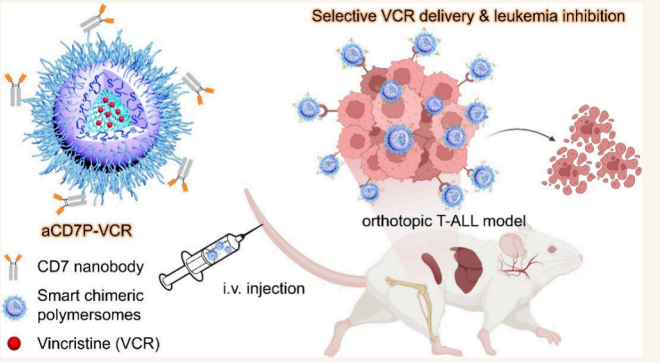

KEYWORDS: *vincristine, targeted drug delivery, leukemia, nanomedicines, chemotherapy*

1. INTRODUCTION

T-cell acute lymphoblastic leukemia (T-ALL), which originates from the abnormal proliferation of malignantly transformed T-cell progenitors, is an aggressive hematological cancer presenting a dismal prognosis.[1−3] With intensive multidrug chemotherapy, including drugs such as vincristine, glucocorticoid and L-asparaginase etc. serving as the standard of care, the response rate has improved for patients who can tolerate these treatments.[4−7] Nevertheless, long-term side effects frequently have a substantial impact on the quality of life of survivors. Moreover, relapse frequently occurs, particularly for adult patients, wherein nearly half of these patients relapse, with fewer than 10% achieving sustained remission and long-term survival.[8−10] The primary reason for such a poor prognosis is the lack of effective salvage options, particularly the absence of targeted therapies in the clinic.[11−13] To date, cytotoxic nelarabine is the only available drug for relapsed or refractory T-ALL patients, but it has serious neurotoxicity and limited efficacy, resulting in a one-year survival rate of less than 30%.[14−17] Safe and effective therapeutic strategies are thus urgently needed.

Ligand-installed nanomedicines have been widely developed to overcome the limitations of chemotherapy and improve therapeutic effects in diverse malignancies via selective delivery to tumor cells and augmenting cellular internalization.[18−21] However, little progress has been made in the treatment of T-ALL because of the lack of suitable surface antigens. A critical target recently identified for T-ALL is CD7, which is a transmembrane glycoprotein highly expressed in more than 95% of T-ALL cases and can mediate rapid cell internalization upon ligand binding.[22−24] Several clinical trials have demonstrated the therapeutic potential of CD7-specific chimeric antigen receptor T (CAR-T) cells in the treatment of relapsed/refractory T-ALL patients, resulting in a high response rate.[25−28]

Herein, we engineered anti-CD7 nanobody-conjugated chimeric polymersomes to enable targeted delivery of vincristine sulfate (aCD7P-VCR), thus potentiating the treatment of orthotopic T-ALL (Figure 1a). Vincristine sulfate (VCR) continues to be a cornerstone of intensive chemotherapy regimens for T-ALL patients due to its ability to

Received: February 25, 2025
Revised: April 17, 2025
Accepted: May 7, 2025

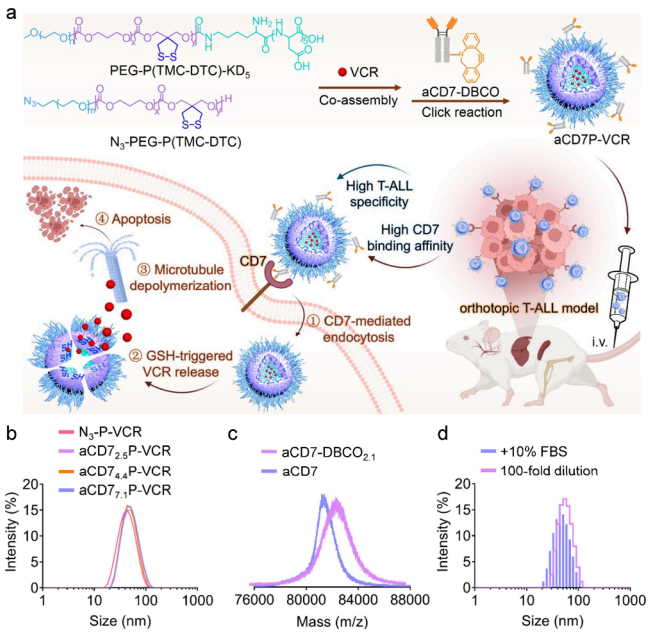

Figure 1. (a) Schematic showing the engineering of anti-CD7 nanobody directed polymersomal vincristine sulfate (aCD7P-VCR) for targeted chemotherapy of orthotopic T-ALL. Created with BioRender.com. (b) Size distributions of N_3-P-VCR and aCD7$_x$P-VCR (x = 2.5, 4.4, 7.1). (c) MALDI-TOF-MS spectra of aCD7-DBCO$_{2.1}$ and aCD7. (d) Size distribution of aCD7P-VCR after incubation with 10% fetal bovine serum (FBS) or 100-fold dilution with HEPES.

disrupt microtubule dynamics and induce cell apoptosis.[29] Notably, aCD7P-VCR with varying aCD7 nanobody densities selectively targeted T-ALL cells, exerting potent inhibition while presenting negligible toxicity against normal T cells. aCD7P-VCR dramatically reduced the leukemia burden in the blood, bone marrow and major organs of orthotopic CCRF-CEM T-ALL-bearing mice, resulting in a significantly greater survival benefit compared with free VCR and nontargeted P-VCR.

2. EXPERIMENTAL SECTION

2.1. Fabrication of aCD7-Modified Polymersomal Vincristine Sulfate (aCD7P-VCR). aCD7P-VCR was prepared by introducing aCD7 to the surface of azide-functionalized P-VCR (N_3-P-VCR) via a strain-promoted click reaction. To facilitate the click reaction, dibenzocyclooctyne-functionalized aCD7 (aCD7-DBCO) was first synthesized via an overnight reaction of aCD7 (110 μL, 2 mg/mL) with a 3-fold molar excess of NHS-PEG$_4$-DBCO (2.7 μL, 2 mg/mL) at 4 °C. aCD7-DBCO was then purified via three rounds of ultrafiltration (MWCO: 10 kDa) using sodium citrate buffer (20 mM, pH 7.4) containing 50 mM sodium chloride. Its DBCO functionality was determined by matrix-assisted laser desorption/ionization time-of-flight mass spectrometry (MALDI-TOF-MS) using native aCD7 as a control. The concentration of aCD7-DBCO was quantified by high-performance liquid chromatography (HPLC) at a wavelength of 214 nm.

N_3-P-VCR was constructed through co-assembly of poly(ethylene glycol)-*b*-poly(trimethylene carbonate-*co*-dithiolane trimethylene carbonate)-*b*-poly(aspartic acid) (PEG-P(TMC-DTC)-KD$_5$, 5.0-(15.0-2.0)-0.8 kg/mol) with N_3-PEG-P(TMC-DTC) (7.9-(15.0-2.0) kg/mol) copolymers (weight ratio of 98:2) and simultaneous electrostatic interaction-driven VCR loading, according to our previous report.[30] To acquire aCD7P-VCR with different aCD7 densities, aCD7-DBCO prepared in advance was added to N_3-P-VCR at aCD7 to N_3 molar ratios of 1:1, 1.5:1 and 2:1 for 36 h of reaction at 4 °C. The mixture was then subjected to three cycles of ultrafiltration (MWCO: 300 kDa) using sterile HEPES buffer (5 mM, pH 7.4). The supernatants were collected to measure the unreacted aCD7-DBCO by HPLC, and the amount and surface density of aCD7 conjugated on the surface of aCD7P-VCR were calculated. The size and size distribution of aCD7P-VCR as well as that after incubation with 10% FBS or following a 100-fold dilution with HEPES, were studied via dynamic light scattering (DLS).

2.2. CD7-Specific Targetability and Endocytosis Studies. The CD7-specific cellular uptake of aCD7P-VCR was investigated in CD7-positive CCRF-CEM T-ALL cells, with CD7-negative 697 B-ALL cells and normal human T cells used as controls. To enable cellular-level visualization, Cy5-labeled polymersomes (aCD7P-Cy5 and P-Cy5) were constructed via incorporation of the Cy5-labeled PEG-P(TMC-DTC) polymer during the course of assembly. For flow cytometry studies, CCRF-CEM cells plated in 6-well plates (2×10^5 cells/well) were cultured with aCD7P-Cy5 bearing different aCD7 surface densities, nontargeted P-Cy5 (Cy5: 27.5 nM) or PBS at 37 °C and 5% CO_2 for 4 h (n = 3). The cells were then centrifuged, rinsed, and suspended in 1× PBS for prompt analysis (BD FACS Calibur). For comparison, 697 cells (2×10^5 cells/well) and human T cells (4×10^5 cells/well) were cultured with aCD7P-Cy5, P-Cy5 or PBS for 4 h and manipulated as described above for analysis.

To investigate the endocytic pathways of aCD7P-Cy5, CCRF-CEM cells (5×10^5 cells/well) were pretreated for 1 h at 37 °C with diverse endocytic inhibitors, including dynasore at a concentration of 80 μM, chlorpromazine hydrochloride (CPZ) at 10 μg/mL, amiloride hydrochloride and methylated β-cyclodextrins (MβCD) at 1 mg/mL. Afterwards, aCD7P-Cy5 was added for a further 1 h of incubation. The cells were subsequently collected, washed and resuspended in PBS for flow cytometry analysis (n = 3). Original CCRF-CEM cells incubated with aCD7P-Cy5 for 1 h were measured to serve as a control.

For confocal laser scanning microscopy (CLSM) studies, CCRF-CEM cells (3.5×10^5 cells/well) were plated into poly-D-lysine-pretreated 24-well plates containing glass slides and cultured for 4 h. Subsequently, the cells were incubated for an additional 4 h with aCD7P-Cy5 or P-Cy5 (Cy5: 21 nM). The cells were then rinsed, fixed with a 4% paraformaldehyde solution for 15 min and stained with 4',6-diamidino-2-phenylindole (DAPI) for 3 min. Finally, microscope slides were prepared by mounting glass slides containing adhered cells for fluorescence imaging using CLSM.

2.3. In Vitro Anti-T-ALL Efficacy of aCD7P-VCR. The in vitro anti-T-ALL effect of aCD7P-VCR was evaluated in CD7-positive CCRF-CEM and Jurkat T-ALL cells via a cell counting kit-8 (CCK-8) assay. 697 B-ALL cells and human peripheral blood mononuclear cells (PBMCs) were used as controls. In brief, CCRF-CEM or Jurkat cells (1.5×10^4 cells/well) seeded in 96-well plates were treated with aCD7$_x$P-VCR, free VCR or nontargeted P-VCR for 48 h. The concentration of VCR ranged from 0.01 to 10.8 nM for CCRF-CEM cells, and from 0.01 to 10 nM for Jurkat cells. Then, 10 μL of CCK-8 solution

https://doi.org/10.1021/polymscitech.5c00030
Polym. Sci. Technol. XXXX, XXX, XXX−XXX

was added, and the mixture was incubated for another 3-5 h. The absorbance of each well at 450 nm was measured with a Varioskan LUX (Thermo Fisher Scientific). Cell viability was determined by comparing the absorbance values to those of control cells incubated with HEPES only (n = 6). The cytotoxicity of $aCD7_{4.4}$P-VCR in 697 cells (1.5×10^4 cells/well, n = 6) and PBMCs (5×10^5 cells/well, n = 3) was similarly evaluated, with P-VCR as the nontargeted control.

2.4. Proapoptotic Effect of aCD7P-VCR on T-ALL. The proapoptotic activity of aCD7P-VCR in CCRF-CEM T-ALL cells was evaluated using an Annexin V-APC/7-AAD apoptosis detection kit. CD7-positive human T cells served as a normal control. CCRF-CEM cells plated in 6-well plates (5×10^5 cells/well) were treated with aCD7P-VCR, free VCR or nontargeted P-VCR for 24 h at a concentration of 2.2 nM VCR. The cells were subsequently harvested, washed twice using PBS and resuspended in 200 μL of 1× binding buffer. The collected cells were stained in the dark with 2 μL of Annexin V-APC and 10 μL of 7-AAD, and then analyzed by flow cytometry. Cells treated with apoptosis positive control solution and HEPES were used as positive and negative controls, respectively.

To corroborate the selectivity and safety of aCD7P-VCR, human T cells in 6-well plates (5×10^5 cells/well) were treated with aCD7P-VCR for 24 h at 0.1, 1.1, 10.8, and 108.3 nM VCR and stained similarly for analysis via flow cytometry.

2.5. Establishment of the Orthotopic CCRF-CEM T-ALL Xenograft Model. All animal procedures were perfomred under protocols approved by Soochow University Laboratory Animal Center and the Animal Care and Use Committee of Soochow University. To establish the orthotopic T-ALL model, female NOD. CB17-*Prkdc*^{scid}/*IL2rg*^{tm1}/Bcgen (B-NDG) mice (6-8 weeks, Biocytogen) were intravenously inoculated with 5×10^5 CCRF-CEM cells each, which is denoted as day 0. On days 3, 6, 12, 24 and 27, blood was withdrawn from the orbital venous plexus of each mouse to monitor leukemia progression. The blood samples were treated with 1× ACK lysis buffer to crack red blood cells, followed by centrifugation and suspension in 1× PBS containing 0.1% FBS. A total of 1×10^6 cells were stained for 15 min using an APC-conjugated anti-human CD45 antibody (1 μL), rinsed with PBS and analyzed by flow cytometry. On day 27, moribund mice were euthanized, and the liver, spleen and hind limbs were harvested for assessment of leukemia infiltration. Tissues were ground into single-cell suspensions and handled similarly to the blood samples for analysis.

2.6. In Vivo Efficacy of aCD7P-VCR in Treating T-ALL. The in vivo efficacy of $aCD7_{4.4}$P-VCR in treating T-ALL was evaluated in orthotopic CCRF-CEM T-ALL-bearing mice. PBS, free VCR and nontargeted P-VCR served as controls. On day 5 post model establishment, the mice were randomly grouped and intravenously administered different VCR formulations every 4 days (Q4D) at 0.25 mg VCR equiv./kg for a total of 5 doses. The weight and status of the mice were periodically monitored during the treatment. Peripheral blood was collected on days 21, 24, and 27 to monitor tumor progression (n = 3).

To further assess the effect of aCD7 surface density on the efficacy of aCD7P-VCR in treating T-ALL, orthotopic CCRF-CEM T-ALL-bearing mice were assigned randomly to different groups on day 3 post tumor inoculation for two cycles of treatment with $aCD7_x$P-VCR (x = 2.5, 4.4, 7.1), P-VCR, free VCR or PBS (n = 8). Four injections (Q3D) at a VCR dosage of 0.25 mg/kg were administered intravenously in each cycle, and there was a one-week interval between the two cycles. The weight and status were periodically monitored. Peripheral blood was collected on days 21, 26, and 31 to monitor tumor progression (n = 3). At the end point of the treatment, 3 mice from each group were randomly sacrificed. The leukemia burden in the liver, spleen, bone marrow and peripheral blood was assessed by flow cytometry. Histological analysis was performed using hematoxylin & eosin (H&E) staining and the samples were examined with an Olympus BX41 microscope. The remaining 5 mice were utilized for survival rate monitoring.

2.7. Statistical Analysis. The data were expressed as the means ± standard deviations and were analyzed using GraphPad Prism 7 software. Statistical comparisons between groups were performed via One-way ANOVA with Tukey's post hoc test. Kaplan−Meier survival curves were generated and compared by the log-rank (Manel-Cox) test. *$p < 0.05$, **$p < 0.01$ and ***$p < 0.001$.

3. RESULTS AND DISCUSSION

3.1. Formation and Characterization of aCD7P-VCR. The development of targeted nanotherapeutics for T-ALL has long been hindered by the lack of specific surface antigens. Recently, CD7 has emerged as a key target for T-ALL, prompting the initiation of several clinical trials exploring CD7-targeted CAR-T therapies.[24] This study aims to develop aCD7 nanobody decorated chimeric polymersomes with a negatively charged cavity to effectively load and selectively deliver VCR (aCD7P-VCR), the frontline cytostatic drug for T-ALL patients, to enable targeted nanochemotherapy of T-ALL. aCD7P-VCR was facilely constructed by clicking an aCD7 nanobody onto the surface of N_3−P-VCR, which was assembled from PEG-P(TMC-DTC)-KD_5 with N_3-PEG-P(TMC-DTC) (98:2 in weight). N_3-P-VCR physically loaded with 4.5 wt % VCR showed a small size of 41 nm and a low polydispersity index (PDI) of 0.08 (Figure 1b, Table 1), which was similar to our previous report and was previously demonstrated to have long-term storage stability and reduction-triggered fast VCR release.[31] To enable the click reaction, the aCD7 nanobody was first reacted with NHS-PEG_4-DBCO at a 3:1 molar ratio, resulting in aCD7-DBCO with an average DBCO functionality of 2.1 (Figure 1c). The click reaction of N_3-P-VCR with aCD7-DBCO at N_3 to aCD7-DBCO molar ratios of 1:1, 1:1.5 and 1:2 yielded $aCD7_x$P-VCR with different aCD7 surface densities (x) of 2.5, 4.4, and 7.1 aCD7 per P-VCR, respectively (Table 1). All $aCD7_x$P-VCR displayed a similar size of 47-48 nm, which was slightly larger than that of the P-VCR (41 nm), and demonstrated a narrow

Table 1. Characterization of $aCD7_x$P-VCR

Polymersomes	aCD7-DBCO to N_3 (feeding molar ratio)	Number of aCD7 per P-VCR[a]	Size (nm)[b]	PDI[b]
N_3-P-VCR	-	-	41	0.08
$aCD7_{2.5}$P-VCR	1:1	2.5	47	0.15
$aCD7_{4.4}$P-VCR	1.5:1	4.4	48	0.21
$aCD7_{7.1}$P-VCR	2:1	7.1	47	0.12

[a]Determined via HPLC. [b]Determined via DLS at 25 °C.

https://doi.org/10.1021/polymscitech.5c00030
Polym. Sci. Technol. XXXX, XXX, XXX−XXX

size distribution (PDI: 0.12-0.21) (Figure 1b, Table 1). We previously verified the vesicular spherical structure of blank P via cryo-TEM.[32] TEM images of aCD7P-VCR further revealed a uniform and spherical structure (Figure S1), with a size close to that determined by DLS. In addition, aCD7P-VCR was robust against either incubation with 10% FBS or 100-fold dilution, showing a negligible change in size distribution (Figure 1d).

3.2. In Vitro Targetability and Selective Anti-T-ALL Activity of aCD7P-VCR. CD7, a T-lineage specific antigen, is largely and commonly overexpressed in T-ALL, making it a promising target under extensive evaluation.[33−36] Here, CD7-positive CCRF-CEM T-ALL cells were employed to assess the T-ALL-specific targetability and antineoplastic activity of aCD7P-VCR, and CD7-negative 697 B-ALL cells and CD7-positive normal human T cells were used as controls. As shown in Figure 2a, the uptake of aCD7P-Cy5 with either 2.5, 4.4, or

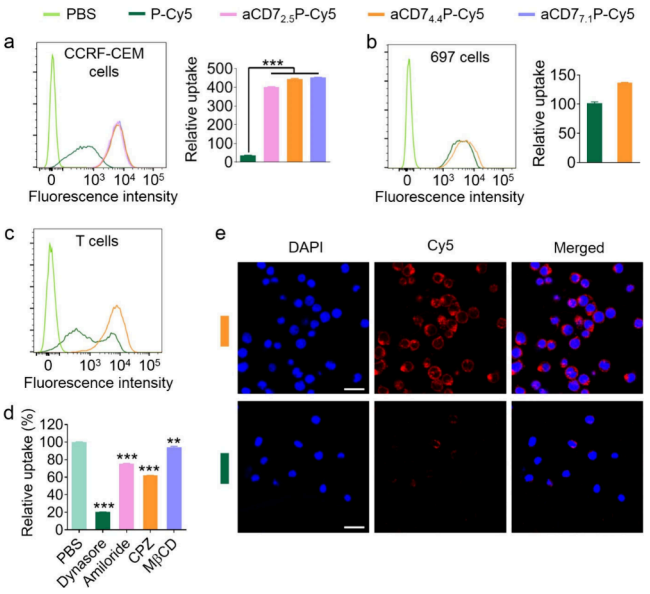

Figure 2. Cellular uptake investigations. (a) Flow cytometry histograms of CCRF-CEM cells after 4 h of incubation with aCD7$_x$P-Cy5 (x = 2.5, 4.4, 7.1), P-Cy5 or PBS, and the corresponding quantitative analysis of Cy5 fluorescence (n = 3). (b) Histograms and quantitative analysis of Cy5 fluorescence in aCD7$_{4.4}$P-Cy5- or P-Cy5-treated 697 cells (n = 3). (c) Cellular association of aCD7$_{4.4}$P-Cy5 and P-Cy5 in normal human T cells following 4 h of incubation. (d) Changes in the cellular uptake of aCD7$_{4.4}$P-Cy5 in CCRF-CEM cells after incubation with different endocytic inhibitors (n = 3). (e) CLSM images of CCRF-CEM cells incubated with aCD7$_{4.4}$P-Cy5 or P-Cy5 for 4 h. Scale bars are 25 μm. $^{**}p < 0.01$, $^{***}p < 0.001$.

7.1 aCD7 on the surface of CCRF-CEM cells was markedly enhanced compared with that of nontargeted P-Cy5, showing a 10.9- to 12.2-fold higher Cy5 fluorescence intensity ($^{***}p < 0.001$). Thereinto, the cellular association of aCD7-P-VCR seemed to reach a plateau as the aCD7 density increased to 4.4, which was utilized for further study in control cells. In CD7-negative 697 cells, the cellular interaction of aCD7$_{4.4}$P-Cy5 was comparable to that of P-Cy5 and was 4.5-fold lower than that in CCRF-CEM cells (Figure 2b). Of note, aCD7$_{4.4}$P-Cy5 exhibited a 1.7-fold lower cellular association in CD7-positive normal T cells than in CCRF-CEM T-ALL cells, despite its higher cellular association relative to that of non-targeted P-Cy5 (Figure 2c).

The uptake pathway of aCD7$_{4.4}$P-Cy5 in CCRF-CEM cells was further studied via the use of diverse endocytic inhibitors to pretreat the cells. The results showed that pretreating cells with CPZ/dynasore clathrin/dynamin inhibitors hindered the internalization of aCD7$_{4.4}$P-Cy5 to the greatest extent, suggesting that receptor-mediated endocytosis is the prime uptake pathway (Figure 2d). In addition, macropinocytosis and caveolae-dependent endocytic pathways also play roles, as evidenced by the significant inhibition of internalization in amiloride- and MβCD-pretreated cells. CLSM images clearly displayed stronger Cy5 fluorescence in aCD7$_{4.4}$P-Cy5-treated CCRF-CEM cells than in cells incubated with P-Cy5 (Figure 2e). These results demonstrated that aCD7 nanobody installation enabled polymersomes to target CD7-positive CCRF-CEM T-ALL cells and boosted their uptake.

The in vitro selective anti-T-ALL activity of aCD7P-VCR was evaluated in CCRF-CEM and Jurkat cells via CCK-8 assays, with 697 B-ALL cells and normal human PBMCs used as controls. Consistent with the results of flow cytometry studies, aCD7P-VCR with any aCD7 density showed higher anti-T-ALL efficacy than P-VCR toward CCRF-CEM cells (Figure 3a). Wherein, aCD7$_{4.4}$P-VCR exhibited the highest

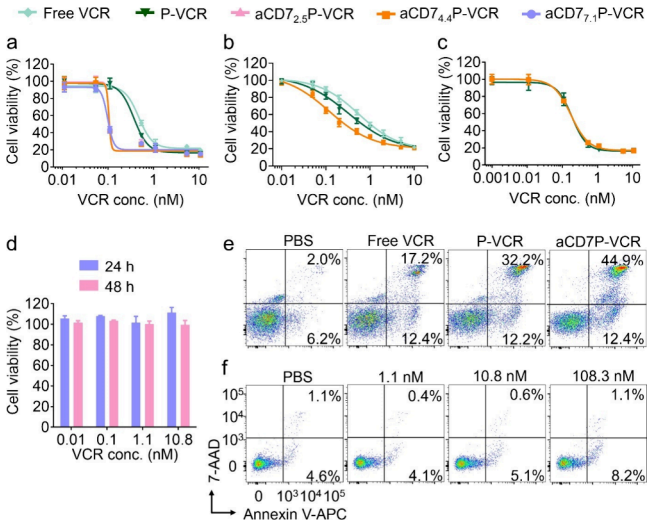

Figure 3. Anti-T-ALL and proapoptotic activity of aCD7P-VCR. Viability of (a) CCRF-CEM cells, (b) Jurkat cells and (c) 697 cells after 48 h treatment with different VCR formulations (n = 6). (d) Cytotoxicity of aCD7$_{4.4}$P-VCR against human PBMCs (n = 3). (e) Apoptosis of CCRF-CEM cells following 24 h incubation with different formulations at 2.2 nM VCR. (f) Apoptosis of human T cells after treatment with aCD7$_{4.4}$P-VCR at different VCR concentrations.

potency with a half-maximal inhibitory concentration (IC_{50}) of 0.11 nM, which was 4.4- and 3.2-fold lower than those of free VCR and P-VCR, respectively. Similar results were also observed in CD7-positive Jurkat cells, in which aCD7$_{4.4}$P-VCR exhibited 4.5- and 2.4-fold stronger anti-T-ALL activity than free VCR and P-VCR (IC_{50}: 0.25 versus 0.94 and 0.61 nM), respectively (Figure 3b). However, in CD7-negative 697 cells, similar cytotoxicity was observed for aCD7$_{4.4}$P-VCR and P-VCR, for which the IC_{50} value (0.23 nM) was 2.1-fold higher than that of aCD7$_{4.4}$P-VCR in CCRF-CEM cells (Figure 3c). Importantly, aCD7$_{4.4}$P-VCR was nontoxic to human PBMCs even at a VCR concentration as high as 10.8 nM (Figure 3d).

VCR, a broad-spectrum antitumor agent, is known to inhibit tubulin polymerization and induce cell apoptosis.[37−40] There-

https://doi.org/10.1021/polymscitech.5c00030
Polym. Sci. Technol. XXXX, XXX, XXX−XXX

fore, we analyzed the proapoptotic effect of aCD7$_{4.4}$P-VCR in CCRF-CEM cells via Annexin V-APC/7-AAD staining, using normal human T cells as a control. As expected, aCD7$_{4.4}$P-VCR caused 57.3% apoptosis in CCRF-CEM cells at 2.2 nM VCR, which was greater than that of free VCR (29.6%) and P-VCR (44.4%) (Figure 3e). It is noteworthy that for normal human T cells, aCD7$_{4.4}$P-VCR did not induce apoptosis at 10.8 nM VCR, and only limited apoptosis was observed at a high VCR concentration of 108.3 nM, showing an apoptosis rate 3.6% higher than that of the PBS group (Figure 3f). It is evident that aCD7P-VCR, which is capable of targeting CD7, potently and selectively inhibited the proliferation of T-ALL cells but had little toxicity to normal human cells.

3.3. In Vivo Therapeutic Efficacy of aCD7P-VCR in Treating T-ALL. To corroborate the efficacy of aCD7P-VCR in treating T-ALL in vivo, an orthotopic CCRF-CEM T-ALL xenograft model was established via injecting CCRF-CEM cells directly into the tail veins of B-NDG mice. Twenty-four days after the model was established, an obvious leukemia burden was observed in the peripheral blood (16.1%), which sharply increased and caused mouse death with a median survival time of 28 days (Figure S2a, b). Furthermore, a severe leukemia burden of over 93% was detected in the bone marrow, liver and spleen (Figure S2c), which was similar to previous reports[41,42] and consistent with the clinical features of T-ALL patients,[43−45] confirming the successful establishment of the orthotopic CCRF-CEM T-ALL model.

On day 5 post inoculation of CCRF-CEM cells, anti-T-ALL treatments were initiated via tail vein injection of aCD7$_{4.4}$P-VCR, free VCR, P-VCR (VCR: 0.25 mg/kg) or PBS for 5 times (Figure 4a). T-ALL progression was effectively inhibited by aCD7$_{4.4}$P-VCR, and the proportion of leukemia cells in the peripheral blood was as low as 0.5% on day 27. However, P-VCR and free VCR only marginally slowed the progression of leukemia cells in the peripheral blood, with the leukemia burden increasing over 12-fold from day 21 to 27 (2.3% to 31.2% and 1.9% to 24.1%), which was 62.4- and 48.2-fold greater than that of the aCD7$_{4.4}$P-VCR group on day 27, respectively (Figure 4b,c). Accordingly, P-VCR or free VCR treated mice displayed a similar median survival time to the PBS group (28 versus 26 days). In contrast, aCD7$_{4.4}$P-VCR treatment provided a significantly better survival benefit than all the other groups and prolonged the median survival to 39 days (Figure 4d, $^{**}p < 0.01$). The weight of mice in all the groups did not significantly change (Figure 4e).

To study the effect of aCD7 density and further improve therapeutic efficacy, two cycles of treatment with aCD7P-VCR bearing different aCD7 densities were performed using nontargeted P-VCR, free VCR and PBS as controls. Four injections were administered at 3-day intervals in each cycle, and there was a one-week rest period prior to the second cycle (Figure 5a). aCD7P-VCR with different aCD7 densities (2.5, 4.4 and 7.1) potently inhibited the proliferation of T-ALL cells, with the leukemia burden in the peripheral blood persistently below 0.4% from days 21 to 31 (Figures 5b and S3). Moreover, the leukemia burden was lower than that in mice following a single cycle of treatment (0.52% on day 27). In comparison, leukemia cells proliferated rapidly in the blood of P-VCR- or free VCR-treated mice, with 2.4-2.6% T-ALL cells on day 21, which increased to 29-34% on day 31, approximately 100-fold higher than those in the aCD7P-VCR groups. Consistently, aCD7P-VCR strongly inhibited T-ALL invasion into the liver, spleen and bone marrow, resulting in a significantly lower

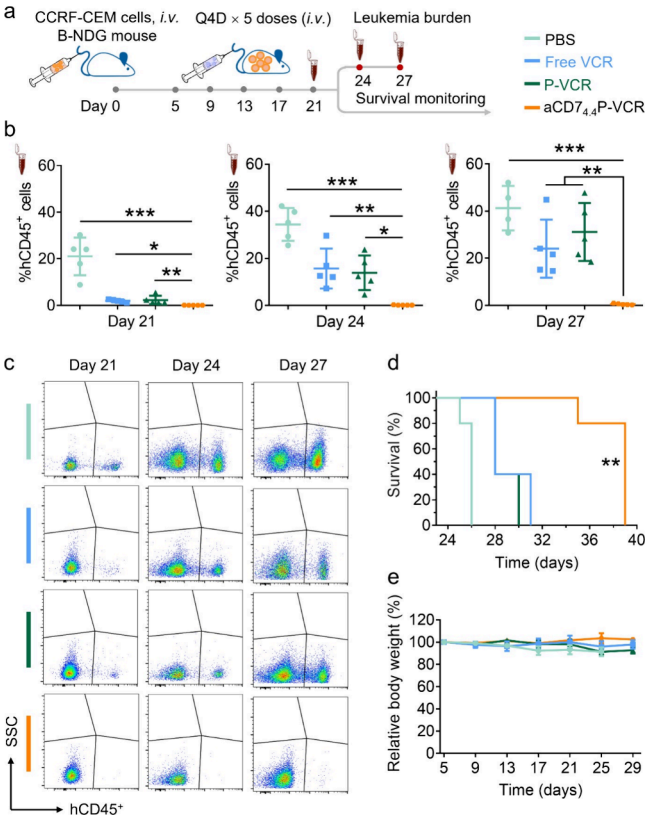

Figure 4. Anti-T-ALL efficacy of aCD7$_{4.4}$P-VCR in orthotopic CCRF-CEM T-ALL-bearing mice. PBS, free VCR and P-VCR served as controls. (a) Treatment and surveillance schedule. (b) Percentages of CCRF-CEM cells in the peripheral blood of different groups at various time points (n = 3) and (c) representative flow cytometry patterns. (d) Kaplan−Meier survival curves and (e) body weight changes in mice treated with different formulations (n = 5). $^*p < 0.05$, $^{**}p < 0.01$, $^{***}p < 0.001$.

leukemia infiltration rate as well as liver and spleen weights than those in all the control groups ($^{***}p < 0.001$, Figure 5c-e). Survival analysis showed that aCD7P-VCR with 2.5, 4.4, or 7.1 aCD7 on the surface substantially improved the survival benefits of mice, with the same median survival time of 43 days, which was significantly longer than free VCR (29 days), P-VCR (31 days) and one cycle of aCD7P-VCR treatment ($^{**}p < 0.01$) (Figure 5f). Of note, the survival benefit of aCD7P-VCR treatment in T-ALL-bearing mice was comparable to that of previously reported CD7-specific CAR-T therapy.[41] All formulations were well tolerated under the therapeutic protocols with no noticeable body weight changes in the mice (Figure 5g).

Histological analysis provided further proof of the significant anti-T-ALL efficacy of aCD7P-VCR, as mice treated with aCD7$_{2.5}$P-VCR, aCD7$_{4.4}$P-VCR and aCD7$_{7.1}$P-VCR all presented normal histomorphology of organs and hind legs with no clear leukemia cells (Figures 6 and S4). This contrasts sharply with P-VCR-, free VCR- and PBS-treated mice, for which substantial leukemia infiltration was observed in the bone marrow, liver and spleen. The abnormal proliferation of leukemia cells within the bone marrow can inhibit normal hematopoiesis, inducing anemia and hemorrhage, which are typical signs in ALL patients.[46,47] As shown by H&E-stained hind limbs, mice treated with PBS, free VCR or P-VCR suffered severe loss of hematopoietic cells in the bone marrow

https://doi.org/10.1021/polymscitech.5c00030
Polym. Sci. Technol. XXXX, XXX, XXX−XXX

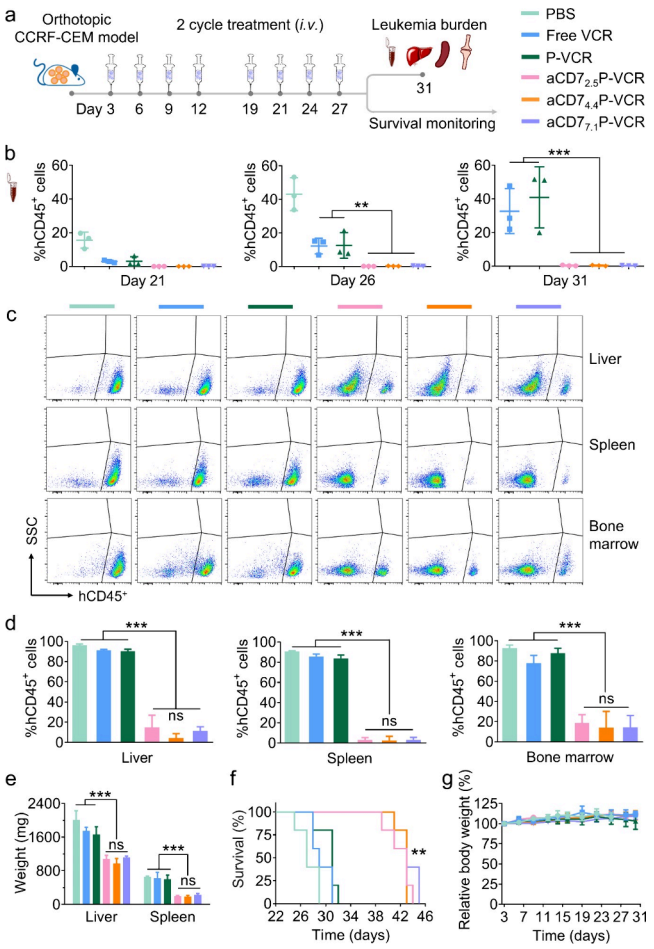

Figure 5. Therapeutic efficacy of aCD7P-VCR in an orthotopic CCRF-CEM T-ALL model. (a) Treatment and surveillance schedule. (b) Percentages of CCRF-CEM cells in the peripheral blood of different groups at various time points (n = 3). (c) Representative flow cytometry pattern and (d) quantitative analysis of CCRF-CEM T-ALL burden in the liver, spleen and bone marrow at the end point of treatment (n = 3). (e) Weights of livers and spleens isolated from mice following different treatments (n = 3). $^{**}p < 0.01$, $^{***}p < 0.001$. (f) Kaplan–Meier survival curves (aCD7$_{2.5/4.4/7.1}$P-VCR versus all other control treatments, $^{**}p < 0.01$) and (g) relative body weights of the mice in different groups (n = 5).

cavity, whereas aCD7P-VCR-treated mice effectively maintained normal hematopoiesis with normal hematopoietic tissue and abundant hematopoietic cells (Figure 6). Taken together, these results confirmed that aCD7P-VCR with different aCD7 densities can selectively target CD7-overexpressing T-ALL cells, leading to significant anti-T-ALL efficacy and survival benefits with good safety.

4. CONCLUSIONS

In this study, we have demonstrated that anti-CD7 nanobody engineered polymersomes enabled targeted delivery of vincristine sulfate (aCD7P-VCR), leading to potent chemotherapy of T-ALL. aCD7P-VCR with controllable aCD7 densities can selectively target and potently inhibit the proliferation of CD7-positive T-ALL cells but does not influence normal T cells. Moreover, aCD7P-VCR, regardless of aCD7 density, effectively reduced the leukemia burden in the orthotopic T-ALL model and provided a significant survival benefit. The CD7 selectivity and high safety of

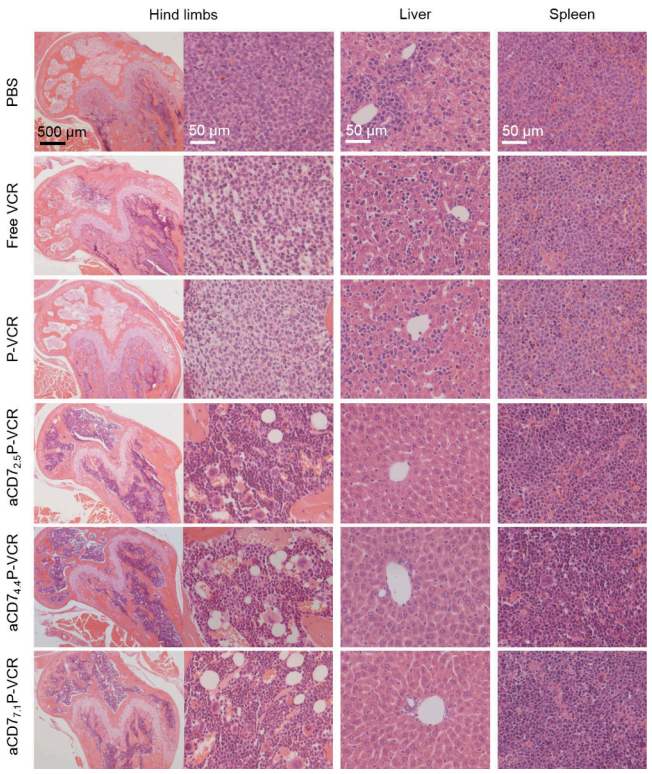

Figure 6. H&E-stained images of hind limbs, liver and spleen collected from mice treated with different formulations.

aCD7P-VCR render it a promising targeted treatment option for T-ALL.

■ ASSOCIATED CONTENT

Supporting Information

The Supporting Information is available free of charge at https://pubs.acs.org/doi/10.1021/polymscitech.5c00030.

Materials; details on characterization; TEM image of aCD7$_{4.4}$P-VCR; establishment of the orthotopic CCRF-CEM T-ALL xenograft model; representative flow cytometry patterns showing the leukemia burden in the blood; H&E-stained images of major organs (PDF)

■ AUTHOR INFORMATION

Corresponding Authors

Zhiyuan Zhong – *State Key Laboratory of Bioinspired Interfacial Materials Science, and Biomedical Polymers Laboratory, College of Chemistry, Chemical Engineering and Materials Science, Soochow University, Suzhou 215123, China; College of Pharmaceutical Sciences, Soochow University, Suzhou 215123, China; International College of Pharmaceutical Innovation, Soochow University, Suzhou 215222, China;* orcid.org/0000-0003-4175-4741; Email: zyzhong@suda.edu.cn

Huanli Sun – *State Key Laboratory of Bioinspired Interfacial Materials Science, and Biomedical Polymers Laboratory, College of Chemistry, Chemical Engineering and Materials Science, Soochow University, Suzhou 215123, China;* orcid.org/0000-0001-6287-1555; Email: sunhuanli@suda.edu.cn

https://doi.org/10.1021/polymscitech.5c00030
Polym. Sci. Technol. XXXX, XXX, XXX–XXX

Authors

Zhenzhen Zhai − *State Key Laboratory of Bioinspired Interfacial Materials Science, and Biomedical Polymers Laboratory, College of Chemistry, Chemical Engineering and Materials Science, Soochow University, Suzhou 215123, China*

Yifan Zhang − *State Key Laboratory of Bioinspired Interfacial Materials Science, and Biomedical Polymers Laboratory, College of Chemistry, Chemical Engineering and Materials Science, Soochow University, Suzhou 215123, China*

Shujing Yue − *State Key Laboratory of Bioinspired Interfacial Materials Science, and Biomedical Polymers Laboratory, College of Chemistry, Chemical Engineering and Materials Science, Soochow University, Suzhou 215123, China*

Fengtao You − *PersonGen BioTherapeutics (Suzhou) Co., Ltd., Suzhou 215100, China*

Lin Yang − *PersonGen BioTherapeutics (Suzhou) Co., Ltd., Suzhou 215100, China*

Complete contact information is available at: https://pubs.acs.org/10.1021/polymscitech.5c00030

Author Contributions

[#]Z. Zhai and Y. Zhang contributed equally to this work. The manuscript was written through contributions of all authors. All authors have given approval to the final version of the manuscript.

Notes

The authors declare no competing financial interest.

■ ACKNOWLEDGMENTS

This work was supported by the National Key R&D Program of China (2021YFB3800900), and the National Natural Science Foundation of China (52273251 and 52473264).

■ REFERENCES

(1) Xu, X.; Zhang, W.; Xuan, L.; Yu, Y.; Zheng, W.; Tao, F.; Nemechek, J.; He, C.; Ma, W.; Han, X.; Xie, S.; Zhao, M.; Wang, J.; Qu, Y.; Liu, Q.; Perry, J.M.; Jiang, L.; Zhao, M. PD-1 Signalling Defines and Protects Leukaemic Stem Cells from T Cell Receptor-Induced Cell Death in T Cell Acute Lymphoblastic Leukaemia. *Nat. Cell Biol.* **2023**, *25* (1), 170−182.

(2) Belver, L.; Ferrando, A. The Genetics and Mechanisms of T Cell Acute Lymphoblastic Leukaemia. *Nat. Rev. Cancer* **2016**, *16* (8), 494−507.

(3) Demoen, L.; Matthijssens, F.; Reunes, L.; Palhais, B.; Lintermans, B.; T'Sas, S.; Fijalkowski, I.; Taminau, J.; Akele, M.Z.; Van Belle, S.; Taghon, T.; Deforce, D.; Van Nieuwerburgh, F.; Berx, G.; Ntziachristos, P.; Debyser, Z.; Durinck, K.; Pieters, T.; Goossens, S.; Van Vlierberghe, P. A Dual Role for PSIP1/LEDGF in T Cell Acute Lymphoblastic Leukemia. *Sci. Adv.* **2024**, *10* (44), No. ea-do6765.

(4) Malard, F.; Mohty, M. Acute Lymphoblastic Leukaemia. *Lancet* **2020**, *395* (10230), 1146−1162.

(5) Lyu, A.; Humphrey, R.S.; Nam, S.H.; Durham, T.A.; Hu, Z.; Arasappan, D.; Horton, T.M.; Ehrlich, L. I. R. Integrin Signaling Is Critical for Myeloid-Mediated Support of T-cell Acute Lymphoblastic Leukemia. *Nat. Commun.* **2023**, *14* (1), 6270.

(6) Patel, J.; Gao, X.; Wang, H. An Update on Clinical Trials and Potential Therapeutic Strategies in T-Cell Acute Lymphoblastic Leukemia. *Int. J. Mol. Sci.* **2023**, *24* (8), 7201.

(7) Teachey, D.T.; O'Connor, D. How I Treat Newly Diagnosed T-cell Acute Lymphoblastic Leukemia and T-cell Lymphoblastic Lymphoma in Children. *Blood* **2020**, *135* (3), 159−166.

(8) Caracciolo, D.; Mancuso, A.; Polerà, N.; Froio, C.; D'Aquino, G.; Riillo, C.; Tagliaferri, P.; Tassone, P. The Emerging Scenario of Immunotherapy for T-cell Acute Lymphoblastic Leukemia: Advances, Challenges and Future Perspectives. *Exp. Hematol. Oncol.* **2023**, *12* (1), 5.

(9) Zhou, Y.; Ji, M.; Xia, Y.; Han, X.; Li, M.; Li, W.; Sun, T.; Zhang, J.; Lu, F.; Sun, Y.; Liu, N.; Li, J.; Ma, D.; Ye, J.; Ji, C. Silencing of IRF8Mediated by M6a Modification Promotes the Progression of T-Cell Acute Lymphoblastic Leukemia. *Adv. Sci.* **2023**, *10* (2), 2201724.

(10) Maciocia, P.M.; Wawrzyniecka, P.A.; Maciocia, N.C.; Burley, A.; Karpanasamy, T.; Devereaux, S.; Hoekx, M.; O'Connor, D.; Leon, T.; Rapoz-D'Silva, T.; Pocock, R.; Rahman, S.; Gritti, G.; Yánez, D.C.; Ross, S.; Crompton, T.; Williams, O.; Lee, L.; Pule, M.A.; Mansour, M.R. Anti-CCR9 Chimeric Antigen Receptor T cells for T-cell Acute Lymphoblastic Leukemia. *Blood* **2022**, *140* (1), 25−37.

(11) Xu, J.; Zhu, H.-H. Targeted Treatment of T-cell Acute Lymphoblastic Leukemia: Latest Updates from the 2022 ASH Annual Meeting. *Exp. Hematol. Oncol.* **2023**, *12* (1), 30.

(12) Bayón-Calderón, F.; Toribio, M.L.; González-García, S. Facts and Challenges in Immunotherapy for T-Cell Acute Lymphoblastic Leukemia. *Int. J. Mol. Sci.* **2020**, *21* (20), 7685.

(13) Xu, J.; Chen, C.; Sussman, J.H.; Yoshimura, S.; Vincent, T.; Pölönen, P.; Hu, J.; Bandyopadhyay, S.; Elghawy, O.; Yu, W.; Tumulty, J.; Chen, C.-h.; Li, E.Y.; Diorio, C.; Shraim, R.; Newman, H.; Uppuluri, L.; Li, A.; Chen, G.M.; Wu, D.W.; Ding, Y.-y.; Xu, J.A.; Karanfilovski, D.; Lim, T.; Hsu, M.; Thadi, A.; Ahn, K.J.; Wu, C.-Y.; Peng, J.; Sun, Y.; Wang, A.; Mehta, R.; Frank, D.; Meyer, L.; Loh, M.L.; Raetz, E.A.; Chen, Z.; Wood, B.L.; Devidas, M.; Dunsmore, K.P.; Winter, S.S.; Chang, T.-C.; Wu, G.; Pounds, S.B.; Zhang, N.R.; Carroll, W.; Hunger, S.P.; Bernt, K.; Yang, J.J.; Mullighan, C.G.; Tan, K.; Teachey, D.T. A Multiomic Atlas Identifies a Treatment-Resistant, Bone Marrow Progenitor-Like Cell Population in T Cell Acute Lymphoblastic Leukemia. *Nat. Cancer* **2025**, *6* (1), 102−122.

(14) Candoni, A.; Lazzarotto, D.; Ferrara, F.; Curti, A.; Lussana, F.; Papayannidis, C.; Del Principe, M.I.; Bonifacio, M.; Mosna, F.; Delia, M.; Minetto, P.; Gottardi, M.; Fracchiolla, N.; Mancini, V.; Forghieri, F.; Zappasodi, P.; Cerrano, M.; Vitale, A.; Audisio, E.; Trappolini, S.; Romani, C.; Defina, M.; Imbergamo, S.; Ciccone, N.; Santoro, L.; Cambò, B.; Iaccarino, S.; Dargenio, M.; Aprile, L.; Chiaretti, S.; Fanin, R.; Pizzolo, G.; Foà, R. Nelarabine as Salvage Therapy and Bridge to Allogeneic Stem Cell Transplant in 118 Adult Patients with Relapsed/Refractory T-cell Acute Lymphoblastic Leukemia/Lymphoma. A Campus All Study. *Am. J. Hematol.* **2020**, *95* (12), 1466−1472.

(15) Shimony, S.; Liu, Y.; Valtis, Y.K.; Paolino, J.D.; Place, A.E.; Brunner, A.M.; Weeks, L.D.; Silverman, L.B.; Vrooman, L.M.; Neuberg, D.S.; Stone, R.M.; DeAngelo, D.J.; Luskin, M.R. Nelarabine Combination Therapy for Relapsed or Refractory T-cell Acute Lymphoblastic Lymphoma/Leukemia. *Blood Adv.* **2023**, *7* (7), 1092−1102.

(16) Śliwa-Tytko, P.; Kaczmarska, A.; Lejman, M.; Zawitkowska, J. Neurotoxicity Associated with Treatment of Acute Lymphoblastic Leukemia Chemotherapy and Immunotherapy. *Int. J. Mol. Sci.* **2022**, *23* (10), 5515.

(17) Shimony, S.; DeAngelo, D.J.; Luskin, M.R. Nelarabine: When and How to Use in the Treatment of T-cell Acute Lymphoblastic Leukemia. *Blood Adv.* **2024**, *8* (1), 23−36.

(18) Gu, W.; Meng, F.; Haag, R.; Zhong, Z. Actively Targeted Nanomedicines for Precision Cancer Therapy: Concept, Construction, Challenges and Clinical Translation. *J. Controlled Release* **2021**, *329*, 676−695.

(19) Mi, P.; Cabral, H.; Kataoka, K. Ligand-Installed Nanocarriers toward Precision Therapy. *Adv. Mater.* **2020**, *32* (13), 1902604.

(20) Rosenblum, D.; Joshi, N.; Tao, W.; Karp, J.M.; Peer, D. Progress and Challenges Towards Targeted Delivery of Cancer Therapeutics. *Nat. Commun.* **2018**, *9* (1), 1410.

(21) Kayani, A.; Raza, A.; Si, J.; Dutta, D.; Zhou, Q.; Ge, Z. Polymersome Membrane Engineering with Active Targeting or Controlled Permeability for Responsive Drug Delivery. *Biomacromolecules* **2023**, *24* (11), 4622−4645.

(22) Gomes-Silva, D.; Srinivasan, M.; Sharma, S.; Lee, C.M.; Wagner, D.L.; Davis, T.H.; Rouce, R.H.; Bao, G.; Brenner, M.K.;

Mamonkin, M. CD7-Edited T cells Expressing a CD7-Specific CAR for the Therapy of T-cell Malignancies. *Blood* **2017**, *130* (3), 285−296.
(23) Li, S.; Wang, X.; Yuan, Z.; Liu, L.; Luo, L.; Li, Y.; Wu, K.; Liu, J.; Yang, C.; Li, Z.; Wang, D.; Shen, L.; Ye, X.; He, J.; Han, C.; Wang, Y.; Zhang, D.; Dong, Y.; Fang, L.; Chen, Y.; Sersch, M.; Cao, W.W.; Wang, S. Eradication of T-ALL Cells by CD7-Targeted Universal CAR-T Cells and Initial Test of Ruxolitinib-Based CRS Management. *Clin. Cancer Res.* **2021**, *27* (5), 1242−1246.
(24) Oh, B. L. Z.; Vinanica, N.; Wong, D. M. H.; Campana, D. Chimeric Antigen Receptor T-cell Therapy for T-cell Acute Lymphoblastic Leukemia. *Haematologica* **2024**, *109* (6), 1677−1688.
(25) Pan, J.; Tan, Y.; Wang, G.; Deng, B.; Ling, Z.; Song, W.; Seery, S.; Zhang, Y.; Peng, S.; Xu, J.; Duan, J.; Wang, Z.; Yu, X.; Zheng, Q.; Xu, X.; Yuan, Y.; Yan, F.; Tian, Z.; Tang, K.; Zhang, J.; Chang, A.H.; Feng, X. Donor-Derived CD7 Chimeric Antigen Receptor T Cells for T-Cell Acute Lymphoblastic Leukemia: First-in-Human, Phase I Trial. *J. Clin. Oncol.* **2021**, *39* (30), 3340−3351.
(26) Ghobadi, A.; Aldoss, I.; Locke, F.L.; Mattison, R.J.; Bhojwani, D.; Maude, S.L.; Dasgupta, P.; Mullis, K.G.; Kabakibi, A.; Hamil, A.S.; Leedom, T.; Chrobak, K.; McNulty, E.; Davidson-Moncada, J.K.; Cooper, M.L.; DiPersio, J.F. A Phase 1/2 Dose-Escalation and Dose-Expansion Study of the Safety and Efficacy of Anti-CD7 Allogeneic CAR-T Cells (Wu-Cart-007) in Patients with Relapsed or Refractory T-Cell Acute Lymphoblastic Leukemia (T-ALL)/ Lymphoblastic Lymphoma (LBL). *Blood* **2021**, *138*, 4829.
(27) Zhang, M.; Chen, D.; Fu, X.; Meng, H.; Nan, F.; Sun, Z.; Yu, H.; Zhang, L.; Li, L.; Li, X.; Wang, X.; Wang, M.; You, F.; Li, Z.; Chang, Y.; Zhou, Z.; Yan, J.; Li, J.; Wu, X.; Wang, Y.; Wang, Y.; Xiang, S.; Chen, Y.; Pan, G.; Xu, H.; Zhang, B.; Yang, L. Autologous Nanobody-Derived Fratricide-Resistant CD7-CAR T-cell Therapy for Patients with Relapsed and Refractory T-cell Acute Lymphoblastic Leukemia/Lymphoma. *Clin. Cancer Res.* **2022**, *28* (13), 2830−2843.
(28) Tan, Y.; Shan, L.; Zhao, L.; Deng, B.; Ling, Z.; Zhang, Y.; Peng, S.; Xu, J.; Duan, J.; Wang, Z.; Yu, X.; Zheng, Q.; Xu, X.; Tian, Z.; Zhang, Y.; Zhang, J.; Chang, A.H.; Feng, X.; Pan, J. Long-Term Follow-up of Donor-Derived CD7 CAR T-cell Therapy in Patients with T-cell Acute Lymphoblastic Leukemia. *J. Hematol. Oncol.* **2023**, *16* (1), 34.
(29) Dhyani, P.; Quispe, C.; Sharma, E.; Bahukhandi, A.; Sati, P.; Attri, D.C.; Szopa, A.; Sharifi-Rad, J.; Docea, A.O.; Mardare, I.; Calina, D.; Cho, W.C. Anticancer Potential of Alkaloids: A Key Emphasis to Colchicine, Vinblastine, Vincristine, Vindesine, Vinorelbine and Vincamine. *Cancer Cell Int.* **2022**, *22* (1), 206.
(30) Zhang, Y.; An, J.; Shao, Y.; Yu, N.; Yue, S.; Sun, H.; Zhang, J.; Gu, W.; Xia, Y.; Zhang, J.; Xu, Y.; Zhong, Z. CD38-Directed Vincristine Nanotherapy for Acute Lymphoblastic Leukemia. *Biomacromolecules* **2022**, *23* (1), 377−387.
(31) Yu, N.; Zhang, Y.; Li, J.; Gu, W.; Yue, S.; Li, B.; Meng, F.; Sun, H.; Haag, R.; Yuan, J.; Zhong, Z. Daratumumab Immunopolymersome-Enabled Safe and CD38-Targeted Chemotherapy and Depletion of Multiple Myeloma. *Adv. Mater.* **2021**, *33* (39), 2007787.
(32) Zhou, C.; Xia, Y.; Wei, Y.; Cheng, L.; Wei, J.; Guo, B.; Meng, F.; Cao, S.; van Hest, J. C. M.; Zhong, Z. GE11 Peptide-Installed Chimaeric Polymersomes Tailor-Made for High-Efficiency EGFR-Targeted Protein Therapy of Orthotopic Hepatocellular Carcinoma. *Acta Biomater.* **2020**, *113*, 512−521.
(33) You, F.T.; Wang, Y.Y.; Jiang, L.C.; Zhu, X.J.; Chen, D.; Yuan, L.; An, G.L.; Meng, H.M.; Yang, L. A Novel CD7 Chimeric Antigen Receptor-Modified NK-92MI Cell Line Targeting T-cell Acute Lymphoblastic Leukemia. *Am. J. Cancer Res.* **2019**, *9* (1), 64−78.
(34) Xie, L.; Ma, L.; Liu, S.; Chang, L.; Wen, F. Chimeric Antigen Receptor T cells Targeting CD7 in a Child with High-Risk T-cell Acute Lymphoblastic Leukemia. *Int. Immunopharmacol.* **2021**, *96*, 107731.
(35) Dai, Z.; Mu, W.; Zhao, Y.; Cheng, J.; Lin, H.; Ouyang, K.; Jia, X.; Liu, J.; Wei, Q.; Wang, M.; Liu, C.; Tan, T.; Zhou, J. T cells Expressing CD5/CD7 Bispecific Chimeric Antigen Receptors with Fully Human Heavy-Chain-Only Domains Mitigate Tumor Antigen Escape. *Sig. Transduct. Target. Ther.* **2022**, *7* (1), 85.
(36) Diorio, C.; Murray, R.; Naniong, M.; Barrera, L.; Camblin, A.; Chukinas, J.; Coholan, L.; Edwards, A.; Fuller, T.; Gonzales, C.; Grupp, S.A.; Ladd, A.; Le, M.; Messana, A.; Musenge, F.; Newman, H.; Poh, Y.-C.; Poulin, H.; Ryan, T.; Shraim, R.; Tasian, S.K.; Vincent, T.; Young, L.; Zhang, Y.; Ciaramella, G.; Gehrke, J.; Teachey, D.T. Cytosine Base Editing Enables Quadruple-Edited Allogeneic CART Cells for T-ALL. *Blood* **2022**, *140* (6), 619−629.
(37) Yue, S.; An, J.; Zhang, Y.; Li, J.; Zhao, C.; Liu, J.; Liang, L.; Sun, H.; Xu, Y.; Zhong, Z. Exogenous Antigen Upregulation Empowers Antibody Targeted Nanochemotherapy of Leukemia. *Adv. Mater.* **2023**, *35* (32), 2209984.
(38) Chao, M.-W.; Lai, M.-J.; Liou, J.-P.; Chang, Y.-L.; Wang, J.-C.; Pan, S.-L.; Teng, C.-M. The Synergic Effect of Vincristine and Vorinostat in Leukemia in Vitro and in Vivo. *J. Hematol. Oncol.* **2015**, *8* (1), 82.
(39) Wordeman, L.; Vicente, J.J. Microtubule Targeting Agents in Disease: Classic Drugs, Novel Roles. *Cancers* **2021**, *13* (22), 5650.
(40) Steinmetz, M.O.; Prota, A.E. Microtubule-Targeting Agents: Strategies to Hijack the Cytoskeleton. *Trends Cell Biol.* **2018**, *28* (10), 776−792.
(41) Chen, D.; You, F.T.; Xiang, S.F.; Wang, Y.Y.; Li, Y.F.; Meng, H.M.; An, G.L.; Zhang, T.T.; Li, Z.X.; Jiang, L.C.; Wu, H.; Sheng, B.J.; Zhang, B.Z.; Yang, L. Chimeric Antigen Receptor T cells Derived from CD7 Nanobody Exhibit Robust Antitumor Potential against CD7-Positive Malignancies. *Am. J. Cancer Res.* **2021**, *11* (11), 5263−5281.
(42) Dong, Y.; You, F.; Zhang, Y.; Sun, H.; Cheng, R.; Zhao, S.; Yang, L.; Zhong, Z. CD7 Nanobody-Based Immuno-Nanotoxin for Targeted Treatment of T-Cell Acute Lymphoblastic Leukemia. *ACS Appl. Nano Mater.* **2024**, *7* (7), 7195−7202.
(43) Zhang, Z.; Yang, K.; Zhang, H. Targeting Leukemia-Initiating Cells and Leukemic Niches: The Next Therapy Station for T-Cell Acute Lymphoblastic Leukemia? *Cancers* **2022**, *14* (22), 5655.
(44) Vadillo, E.; Dorantes-Acosta, E.; Pelayo, R.; Schnoor, M. T Cell Acute Lymphoblastic Leukemia (T-ALL): New Insights into the Cellular Origins and Infiltration Mechanisms Common and Unique among Hematologic Malignancies. *Blood Rev.* **2018**, *32* (1), 36−51.
(45) Litzow, M.R.; Ferrando, A.A. How I Treat T-cell Acute Lymphoblastic Leukemia in Adults. *Blood* **2015**, *126* (7), 833−841.
(46) Hunger, S.P.; Mullighan, C.G. Acute Lymphoblastic Leukemia in Children. *N. Engl. J. Med.* **2015**, *373* (16), 1541−1552.
(47) Moribe, T.; Xu, L.; Tajima, K.; Yonemoto, N. Real-World Treatment Patterns of Novel Drugs in Relapsed or Refractory Acute Lymphoblastic Leukemia Patients in Japan. *Future Oncol.* **2023**, *19* (19), 1343−1356.

https://doi.org/10.1021/polymscitech.5c00030
Polym. Sci. Technol. XXXX, XXX, XXX−XXX